



A comprehensive study of ultrafast carrier dynamics of LT-GaAs: Above and below bandgap regions



Nikita Vashistha ^{a,b}, Mahesh Kumar ^{a,b,*}, Rajiv K. Singh ^{a,b}, Debiprasad Panda ^c, Lavi Tyagi ^{c,d}, Subhananda Chakrabarti ^c

^a CSIR-National Physical Laboratory, Dr. K.S. Krishnan Road, New Delhi, 110012, India

^b Academy of Scientific and Innovative Research, AcSIR Headquarters, Ghaziabad, Uttar Pradesh, 201002, India

^c Dept. of Electrical Engineering, IIT Bombay, Mumbai, 400076, India

^d Center for Research in Nano Technology and Science, IIT Bombay, Mumbai, 400076, India

ARTICLE INFO

Keywords:

Ultrafast transient absorption spectroscopy
Band filling
Bandgap renormalization
Lifetime
Trap time

ABSTRACT

We report the study of ultrafast carrier dynamics of low temperature grown GaAs over wide spectral range (2.75 eV–0.88 eV) with above and below bandgap (E_g) optical excitations using ultrafast transient absorption spectroscopy. The presence of defects and their subsequent effect on the pathway and lifetime of carrier relaxation with probing at different energy levels is presented. The carrier relaxation pathways and their corresponding models are predicted. It is observed that for pumping (2.58 eV) and probing above E_g , the transient behavior is dominated by band filling while renormalization is in prominence when probed near to E_g . For below E_g pumping (0.88 eV) the optical behavior is mostly governed by defects. The calculated trap time is in the range of ~128 fs to ~807 fs while overall recombination time shows a wide variation from ~1.38 ps to ~1.25 ns depending on the position of traps/defects in the forbidden band.

1. Introduction

III-V semiconductors have been studied for quite a while for their fascinating optoelectronic properties. GaAs is one such compound semiconductors which have made quite a special place in optoelectronics [1–3] and photovoltaics [1,4,5] fields because of its exotic optical properties that can be tuned with growth conditions and post-growth annealing [6–12]. Besides, GaAs grown at low growth temperature (190 °C–300 °C) has emerged out to be unstoppably demanding and prestigious component of the GaAs industry [13–15]. This low-temperature GaAs (LT-GaAs) is known to have carrier lifetimes in sub-picosecond duration and carrier trapping happens in few femtoseconds only [10,14] making them the material of choice for applications like photoconductive switches, THz emitter/detectors and saturable absorbers [13–16].

The study of this kind of epitaxial films grown by molecular beam epitaxy was firstly done for investigating the substrate temperature dependence during growth [17]. A low-temperature growth along with excess group V atoms results in the formation of point defects like antisites, interstitials, vacancies and other complex local defects [18,19]

that lie in the forbidden gap (Fig. 1). These defects result in fast trapping, which reduces carrier concentration and leads to semi-insulating properties [14]. So, these films exhibit resistivity in the range of ~ 10^4 - 10^6 Ω·cm [18,20]. A decrease in resistivity happens when there is conduction by hopping of electrons between antisites [11,21]. A low trapping time because of the defects ensures fast switching in photoconductive switches while a fast relaxation time from these defects results in quick recovery in saturable absorbers [9]. Apart from this, the introduction of these high resistive low temperature grown layers in FETs reduces the back-gating, side gating and light sensitivity problems [11,14,18,22].

The presence of defects and crystallinity of such a thin film is a cumulative function of growth temperature [23], As/Ga flux ratio and growth rate. Generally, layers grown above 200 °C, show monocrystalline nature with no line or extended defects [18,23]. However, no crystallinity is observed for those grown below 200 °C due to the formation of structural defects like dislocations, stacking faults, and micro twins [23–25]. At 200 °C growth temperature and with Arsenic (As) overpressure, As antisites (As_{Ga}) emerge as dominant (point) defect [11, 12,19], that forms a donor level near to the center of bandgap as shown in Fig. 1. Some tail states arising from structural or impurity defects will

* Corresponding author. CSIR-National Physical Laboratory, Dr. K.S. Krishnan Road, New Delhi, 110012, India.

E-mail address: mkumar@nplindia.org (M. Kumar).

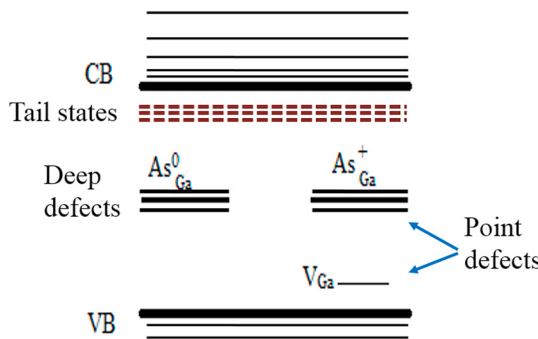


Fig. 1. Schematic energy level diagram showing the defect states of LT-GaAs grown in an Arsenic rich environment.

be present near the conduction band (CB) edge. If the growth temperature is reduced below 200 °C a further lowering in the lifetime will occur because of the incorporation of more defects, both structural and point defects [26].

The As_{Ga} point defect is a double donor, generally found in its neutral (As_{Ga}⁰) and charged state (As_{Ga}⁺) [9]. The positively charged defect states act as electron traps (similar to EL2 defects of semi-insulating GaAs) [11, 18, 27, 28]. These are compensated by native acceptors which in the case of LT-GaAs are Gallium vacancies (V_{Ga}) [9], thus, giving rise to electron-deficient states (As_{Ga}⁺) at the mid-gap region. The concentration of these antisites is an inverse function of growth temperature [9, 29], because of which fast trapping is observed at lower growth temperatures but there is an inverse effect on trap emptying time [30]. At a low growth temperature of 200 °C, the typical concentrations are reported as high as As_{Ga}⁰ ≈ 10²⁰ cm⁻³ and As_{Ga}⁺ ≈ 10¹⁹ cm⁻³ [11, 31].

The acceptor vacancies (V_{Ga}) form a band near to the valence band (VB) and have a concentration equal to As_{Ga}⁺ [29, 32]. These mid-bandgap states act as non-radiative recombination centers that decrease the carrier lifetime and resistivity due to fast trapping and hopping conduction in the donor level, respectively. Despite this high concentration of defects LT-GaAs has been reported to have high mobility (~200 cm²/Vs) [33].

To understand the optical behavior of LT films there are many studies [9, 29–38] revealing the carrier dynamics but these are mostly focussed on near bandgap excitations and single probing states. Some of the studies include the effect of trap states or defects on lifetime as well [10, 33, 38] but are mostly reported with significant contribution from VB. In this work, we have studied changes in carrier lifetime and carrier trapping behavior in LT-GaAs thin films at different probing energies (ranging from 0.88 eV to 2.75 eV) using ultrafast transient absorption spectroscopy (UFTS) with below (0.88 eV) and above (2.58 eV) the bandgap optical excitations (Fig. 2). The behavior of carriers in the energy state from 2.75 eV to 0.88 eV was captured. The technique enabled measurements of trapping and recombination lifetime in a time scale varying from few femtoseconds (fs) to few nanoseconds (ns). The trajectory of decay of these hot carriers from CB in the presence of defect states also focuses on their scattering dynamics, since at low concentration level, this relaxation is governed by electron-phonon coupling [39]. Probing above and around the bandgap of LT-GaAs reveals the dynamics of hot carrier coulomb interactions especially band filling and bandgap renormalization [40], while probing below the bandgap, the distribution and contribution of defects on carrier lifetime and optical behavior of LT-GaAs is revealed. With excitation at 0.88 eV, the mid-gap states are directly addressed. The behavior may also result into significant two-photon absorption (2 PA) which will be dependent on the fluence of the pump beam. For this study, we have kept the fluence as minimum as possible so that the 2 PA effect is not dominant. For the above band excitation, the spectra and transient behavior will depict the behavior of CB states. The prime focus of this study is to identify the most probable pathways followed by the excited electrons and the

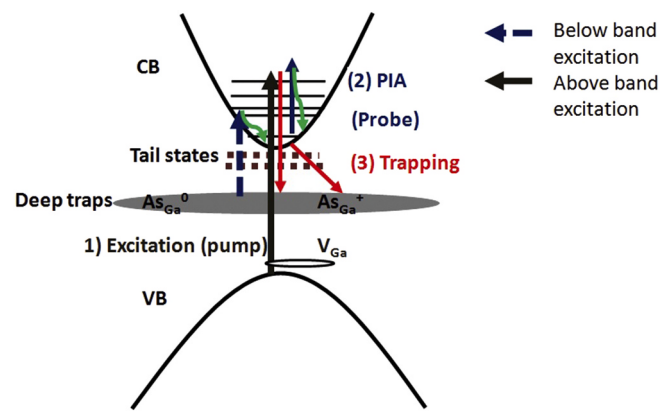


Fig. 2. LT-GaAs under optical excitation in transient absorption spectroscopy. It shows (1) how carriers are excited to conduction band by pump beam (blue dashed arrow: below bandgap, black solid arrow: above bandgap) (2) excited state absorption (ESA) by probe i.e. probe induced absorption (PIA) (3) decay to and trapped by traps lying near to CB and the mid of bandgap. The green arrow shows vibrational relaxation or internal conversion. (For interpretation of the references to colour in this figure legend, the reader is referred to the Web version of this article.)

determination of the CB states which give the fastest trap time. The trapping time, recombination time and origin of carriers are stated clearly over a broad region of study (2.75 eV–0.88 eV).

2. Material and methods

The sample investigated was grown by molecular beam epitaxy (MBE) on a semi-insulating GaAs substrate under excess Arsenic flux with As/Ga flux ratio taken as 10. For the growth, the interaction of Gallium and Arsenic species and their subsequent impingement over a heated GaAs substrate is required. For this study, As₄ molecules and Gallium atoms were used as constituents. The growth cycle consisted of two steps. At first, a 600 nm buffer layer of GaAs is deposited at 590 °C followed by a 45 nm thick LT-GaAs film at 200 °C by migration enhanced epitaxy method. No subsequent annealing was performed to study the defect induced carrier dynamics. Ultrafast transient absorption spectroscopy (UFTS) was performed using a Ti:Sapphire based femtosecond laser system comprising of an oscillator (Micra by Coherent), amplifier (Legend by Coherent), OPA (by Light Conversion) and spectroscopy system (Helios by Ultrafast Systems). The 3.5 mJ output of the amplifier with a pulse width of 40 fs centered at 800 nm was split into two parts. One part was fed to the OPA with 1.75 mJ energy, and the other part with 0.5 mJ energy was fed to the spectrometer through a delay stage capable of introducing a delay of 0–8 ns. Broadband white light was generated inside the spectrometer by passing the lower energy split beam through a sapphire plate which can generate probe pulses of 3.54 eV–0.775 eV energy through a combination of crystals. The stable outputs of OPA at 2.58 eV and 0.88 eV were chosen to excite (pump) the sample below and above the bandgap regions. The average power (pulse energy) of the pump was ~1.5 mW (3 µJ). Surface Xplorer software and Origin 9.1 were used for the analysis and kinetics fitting. The system was calibrated using the ZnTPP dye, while the wavelengths were calibrated (traceability provided by the Optical metrology group of NPL India) using the calibrated Ocean Optics spectrometer. The same laser source was used to study the non-linear absorption using Z-scan technique. The mobility and resistivity are measured through Hall-Effect measurement while the presence of strain in the film and generation of phonons and layer crystallinity is shown through Raman (HORIBA, T64000) and GI-XRD(PANalytical X'Pert PRO MRD high-resolution XRD system). A Hall measurement was done at room temperature with current 7.8 nA and magnetic field as 5k Tesla, using HEMS from nano-magnetics. Raman measurement was using a triple monochromator having a 514.5 nm

excitation source. The thickness of the LT film grown was calculated through ellipsometry (J.A. Wollem Ellipsometer VASE). Band to band transitions confirming the bandgap and defect state transitions were measured by UV-Vis-NIR spectroscopy (Agilent Technologies, Cary 5000i). The presence of non-linear behaviour (non-linear absorption) in the NIR range in the sample was confirmed through Z-scan.

3. Results and discussion

Table 1 one depicts the mobility and resistivity values for LT-GaAs measured through Hall effect measurement. The experiment was repeated twice at 295 K to see whether the values are consistent. The variation was minute and on average the mobility and resistivity values were approximately $\sim 144 \text{ cm}^2/\text{V}\cdot\text{s}$ and $\sim 2.53 \times 10^3 \Omega\cdot\text{cm}$, respectively. Since both the values are low, it indicates a high concentration of defects that provide a hindrance in a free flow of carriers thus, affecting the mobility and decreasing the resistivity by hopping conduction.

The Raman spectrum reveals two phonon peaks as shown in Fig. 3(a) at 269 cm^{-1} (8.03 THz) and 292.6 cm^{-1} (8.77 THz). The first peak corresponds to phonon which arises due to scattering from crystalline disorder normal to the surface while second peak is of LO phonon at the critical point Γ located at the center of Brillouin zone [20] corresponding to Γ_{15} -LO phonon frequency in crystalline GaAs (8.78 THz). The presence of TO phonon indicates the presence of defects in the film. The shift in LO and TO peaks from the reported value of 268 cm^{-1} and 291 cm^{-1} [12] can be either due to tensile strain (due to excess As) [36] or compressive strain (due to substrate) [28]. Since we have observed a blue shift ($\sim 0.34 \text{ cm}^{-1}$ (0.01 THz)) in energy it indicates the presence of tensile strain or expansion of lattice in the LT-GaAs layers due to the incorporation of excess Arsenic. This suggests that the LT-GaAs films need post-growth annealing to release this strain [29,34]. These phonons will assist in the decay of optically excited carriers through the coupling of energy with lattice [41,42]. The effective penetration depth of the electromagnetic field of laser in Raman is calculated by the following formula [20].

$$\delta = \frac{\lambda}{2\pi k} \quad (1)$$

Where λ is Raman wavelength used for measurement and k is the extinction coefficient corresponding to λ . From ellipsometry measurement (Fig. 5(a)), value of k comes out to be 0.778. This value when substituted in equation (1) gives penetration depth as $\sim 105 \text{ nm}$. This implies that the spectrum obtained through Raman carries information about the GaAs buffer layer as well (Fig. 3(a)). The GI-XRD (Fig. 3(b)) result shows two diffraction peaks one at 53.3° corresponding to LT-GaAs epitaxial layer and other at 53.7° from (311) cubic plane of GaAs. The crystallite size around 53.3° is 31.9 nm .

From UV-Vis-NIR spectroscopy (Fig. 4(a)) a broad absorption above the band edge is obtained. The Tauc plot (Fig. 4(b)) gives the value of direct bandgap (E_g) as 1.46 eV (849 nm). In semi-insulating materials, the residual absorption (Urbach tail) below bandgap is due to the formation of localized states associated with defects/disorder or impurities or low crystallinity [43,44]. In LT-GaAs it is governed by isolated neutral As_{Ga} antisites [27]. This residual absorption, when fitted with Urbach empirical formula [42], will give Urbach energy, $E_u = 1.16 \text{ eV}$ (1068.9 nm).

The thickness of LT-GaAs film is calculated to be $\sim 43 \text{ nm}$ by ellipsometry (mean squared error = 0.811) by fitting refractive index (n) and

extinction coefficient (k) values (Fig. 5(a)). The thickness values are well within the measurement error. Slight difference ($\sim 2 \text{ nm}$ and less) in thickness value obtained from piezo sensors in MBE system (45 nm) and ellipsometry data ($\sim 43 \text{ nm}$) is due to the measurement error in piezo sensor of MBE or due to the model fitting in ellipsometry data. Z-scan in open aperture mode (Fig. 5(b)) was performed under 800 nm (NIR) pulsed femtosecond duration laser irradiation having peak power (around focus) of about $4.3 \times 10^{10} \text{ W/cm}^2$. The fitting was with an agreement with two-photon absorption (2 PA) and the non-linear absorption coefficient (β) came out to be $2.4 \times 10^{-10} \text{ cm/W}$. The 2 PA coefficient i.e. β for n-GaAs and undoped GaAs using a picosecond duration Nd-glass laser ($1 \mu\text{m}$) has been reported to be in $\sim 10^{-8} \text{ cm/W}$ range [45,46]. 2 PA will be a dominant absorption process in GaAs for the 0.73 eV - 1.38 eV (900 nm-1700 nm) range [45]. With femtosecond laser and 800 nm wavelength, 2 PA value of LT-GaAs is less than that for picosecond laser with 1000 nm wavelength. It indicates that 2 PA will not govern the behavior of LT-GaAs with 2.58 eV (480 nm) excitation (above band edge) and a visible probe. However, for 0.88 eV (1400 nm) excitation (below band edge) and NIR probe, 2 PA will be present but the contribution will be insignificant as value of β is very low ($2.4 \times 10^{-10} \text{ cm/W}$) for LT-GaAs in the region of study.

Figs. 6(a) and 7(a) shows the difference absorption spectra of LT-GaAs excited by 2.58 eV (480 nm) excitation pulse (pump). The pump energy exceeds the bandgap ($\sim 1.46 \text{ eV}$) for the material. The data was collected using a broad probe in the visible range (2.75 eV-1.55 eV) as well as in near IR range (1.55 eV-0.88 eV). Excitation at lower energy i.e. with 0.88 eV pump is shown in Fig. 8(a). The corresponding kinetics at different probing energies is shown in Figs. 6(b), 7(b) and 8(b), respectively. The transient behavior is recorded over a wide time range (0-5 ns). Models predicting the probable pathways with corresponding trap times (t_1) and trap emptying time (t_2 and t_3) are distinctively mentioned at different probe ranges (Figs. 9-11).

Since the band to band absorption in GaAs falls in the near-infrared range ($\sim 849 \text{ nm}/1.46 \text{ eV}$) so the spectrum in visible range will lack any information about it. However, in NIR range as shown in Figs. 7(a) and 8(a) a small dip was observed near 849 nm corresponding to VB-CB transition ($S_0 - S_1$) which is a transient state and occurs for few femtoseconds. The strength of this peak indicates that this band to band transition was induced by probe beam and screened by a huge density of electrons present at the CB edge. A broad probe-induced absorption (PIA) corresponding to excited-state absorption (ESA) covering the whole visible and NIR range is observed which is an indicator of density of carriers in excited states of CB. There is an increase in this absorption near to band (below 1.65 eV) after 250 fs (Fig. 6(a)) because of probe induced re-absorption of thermally relaxed carriers from states near to the CB minima.

With 2.58 eV (Fig. 7(a)) excitation the NIR spectra beyond 1.24 eV show a continuous rise in PIA after 1.5 ps. These transitions are either from defect states or internally within the CB states. However, this behavior was not seen when excitation was changed to 0.88 eV (Fig. 8(a)). The density of excited carriers was almost constant with a broad dip near 1.24 eV (1000 nm) (after 5 ps) showing a possibility of transition of electrons between vibrational states belonging to two different electronic singlet states. The broadness is due to the overlapping of these vibronic states in thin films. A lower density of carriers in CB (from the magnitude of difference absorption in Fig. 8) is due to the excitation far below the E_g . Around 1.46 eV we can see ESA up to 5 ps followed by a negative peak persistent up to 10 ps. This is a probe mediated ground state bleach (GSB) ($S_0 - S_1$ transition) dominated by ESA. This ESA region is important as it carries information about the relaxation trajectory of carriers in CB states. By probing them at different wavelengths, the lifetime of decay of these excited carriers can be calculated and the relaxation pathways can be determined. This pathway is studied through the kinetic profile (Figs. 6(b), 7(b) and 8(b)) while probing part of spectra with significant changes in the spectral profile. A kinetic profile is fit by the following equation to calculate lifetime [47].

Table 1
Resistivity and mobility values for LT-GaAs through Hall Effect measurement.

S.no.	Temperature (K)	Resistivity ($\Omega\cdot\text{cm}$) ($\times 10^3$)	Mobility ($\text{cm}^2/\text{V}\cdot\text{sec}$)
1	295	2.53	145
2	295	2.54	143

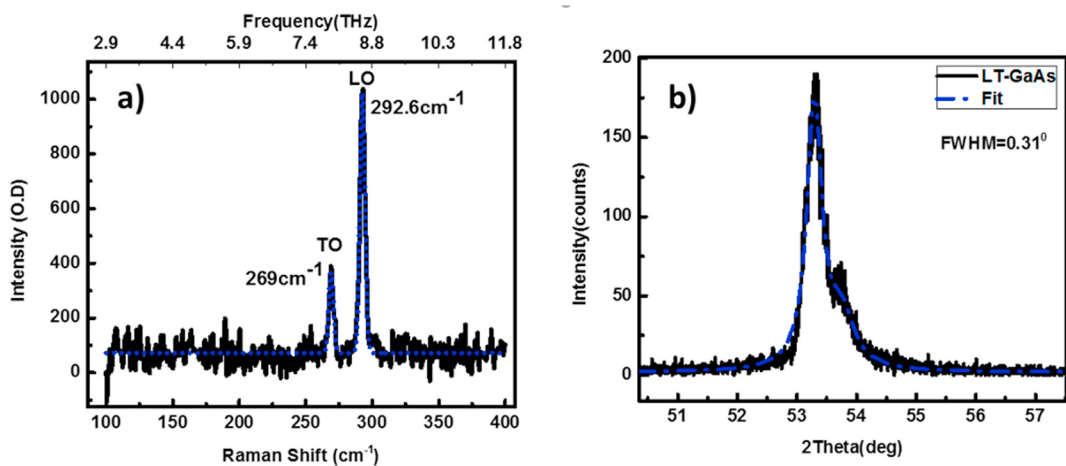


Fig. 3. Showing (a) Raman spectrum and (b) GI-XRD of LT-GaAs.

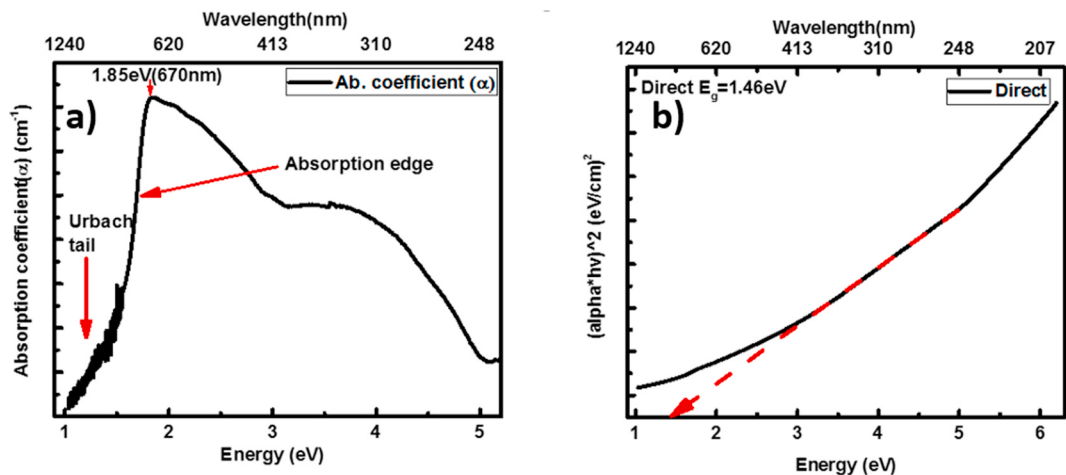


Fig. 4. a) Steady state absorption of an LT-GaAs sample and b) Tauc plot depicting direct bandgap of LT-GaAs.

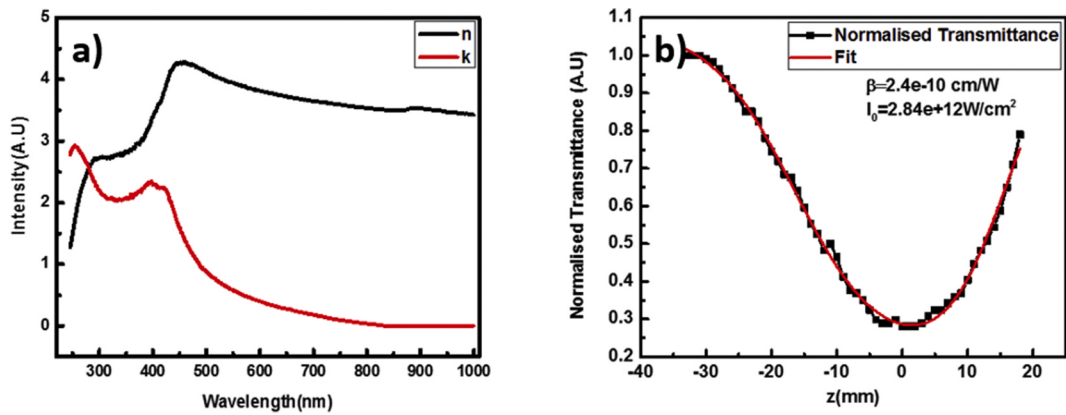


Fig. 5. a) n and k values of LT-GaAs obtained through ellipsometry and b) plot of normalised transmittance wrt delay z obtained from open aperture Z-scan.

$$\mathbf{C}_i^*(\mathbf{t}) = \mathbf{IRF}^* \mathbf{C}_i \quad (1)$$

$$\mathbf{C}_i^*(\mathbf{t}) = e^{-\left(\frac{t-t_0}{t_p}\right)^2} * \sum_i A_i e^{-\left(\frac{t-t_0}{t_i}\right)} \quad (2)$$

Here, IRF is instrument response function, C_i undistorted draw kinetic profile, C_i^* is the convolved output, t_p is FWHM of IRF, t_0 is time

zero while A_i and t_i are contribution of i th component and decay time (time constant or lifetime) of i th component respectively. The decay time or lifetime (t_i) is an average time in which charge carriers having A_i contribution annihilate (recombine or get trapped in trap states). The kinetic fit (for a particular probe energy) using equation (2) yields a series of t_i s each with corresponding A_i . The value of integer "i" which indicates number of significant components in decay kinetics, is

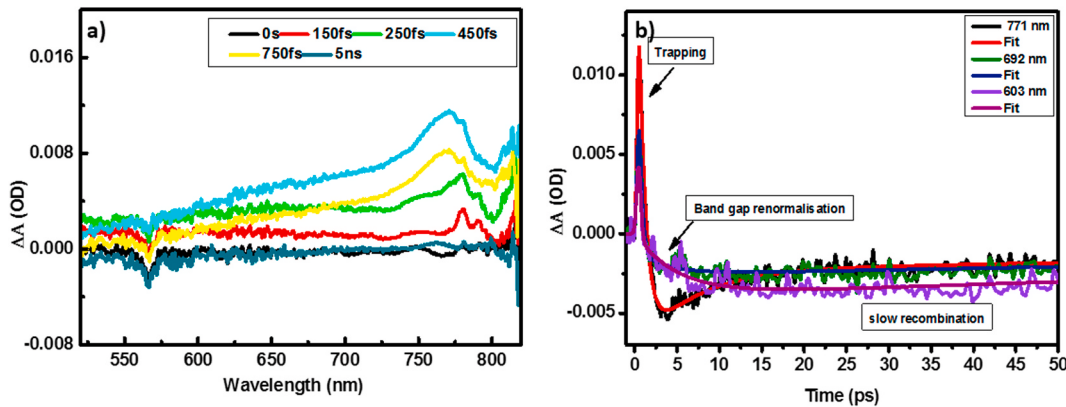


Fig. 6. (a) Difference absorption spectra of LT-GaAs depicting evolution and decay of broad PIA and (b) decay kinetics of LT-GaAs sample corresponding to a chosen probing state captured under 2.58 eV pump excitation (1.5 mW average power) and a visible probe. The decay kinetics show the signature of trapping process, bandgap renormalisation and slow recombination.

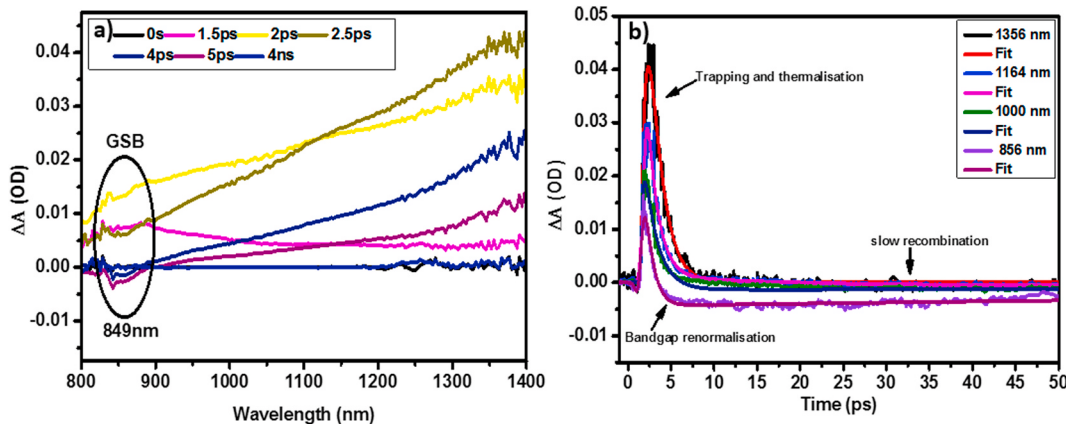


Fig. 7. (a) Difference absorption spectra of LT-GaAs depicting appearance of GSB and evolution and decay of broad PIA and (b) decay kinetics of LT-GaAs sample corresponding to a chosen probing state captured under 2.58 eV pump (1.5 mW average power) and a NIR probe. The decay kinetics indicates the prominace of bandgap renormalization for near band edge states.

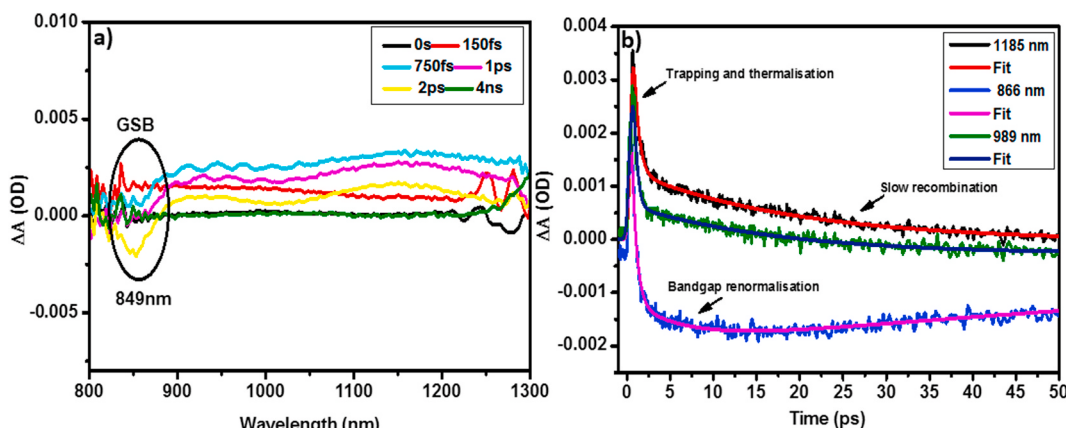


Fig. 8. (a) Difference absorption spectra of LT-GaAs depicting appearance of GSB and evolution and decay of broad PIA and (b) decay kinetics of LT-GaAs sample corresponding to a chosen probing state captured under 0.88 eV pump (2 mW P_{avg}) and NIR probe. The absorption and kinetic behaviour at this excitation is as a result of defect states.

preferred to be ≤ 3 .

The closeness of fit is given by standard deviation (σ) value calculated as following

$$\sigma = \sqrt{\sum \frac{(S_{exp} - S)^2}{n - 1}} \quad (3)$$

Where S is raw signal, S_{exp} is the fitting signal and n is the number of data

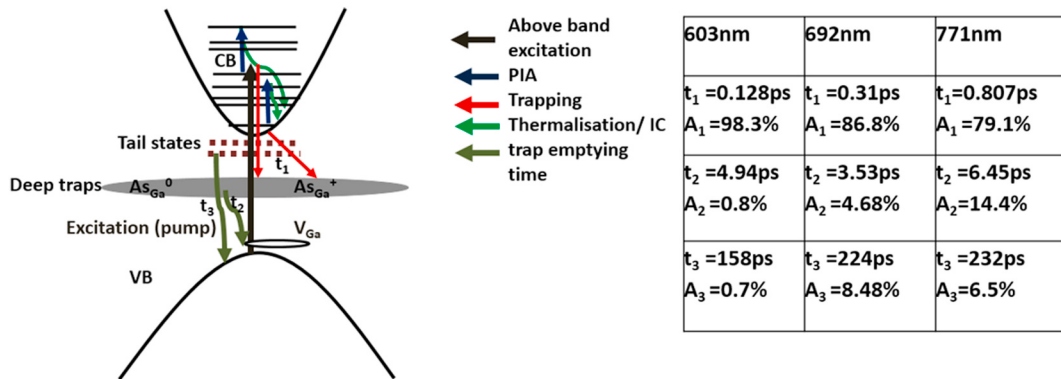


Fig. 9. LT-GaAs under above band excitation and visible probe in transient absorption spectroscopy. Time constants for 2.58 eV excitation and visible probe are listed on the table on right. The column header corresponds to probing wavelengths at which decay kinetics is analysed and the subsequent row entries (t_1, t_2, t_3, A_1, A_2 and A_3) are the fitting coefficients for the kinetic behaviour that gave the best fit.

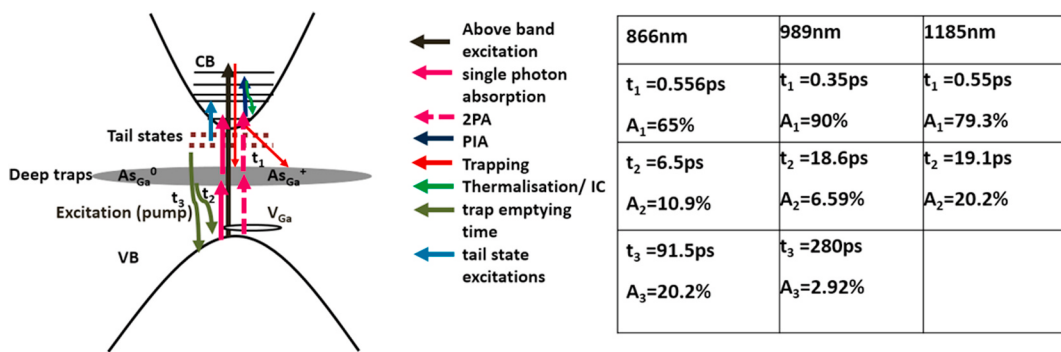


Fig. 10. LT-GaAs under (2.58 eV) above band excitation and NIR probe in transient absorption spectroscopy. The column header corresponds to probing wavelengths at which decay kinetics is analysed and the subsequent row entries (t_1, t_2, t_3, A_1, A_2 and A_3) are the fitting coefficients for the kinetic behaviour that gave the best fit.

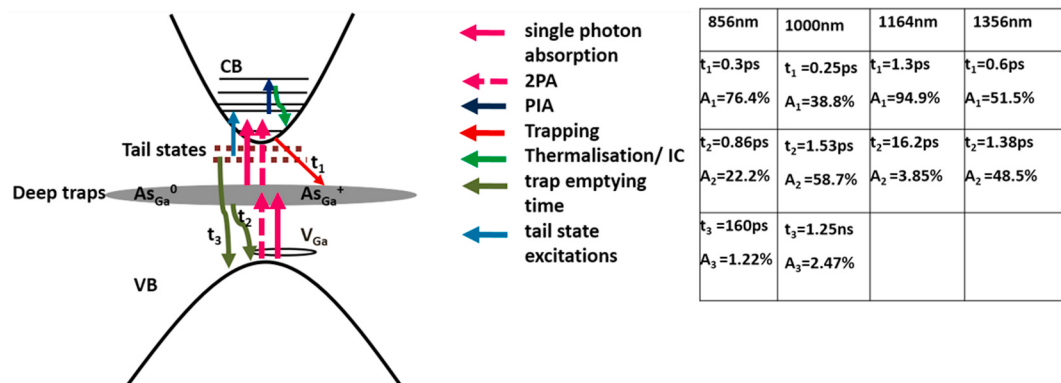


Fig. 11. LT-GaAs under (0.88 eV) below band excitation and NIR probe in transient absorption spectroscopy. The column header corresponds to probing wavelengths at which decay kinetics is analysed and the subsequent row entries (t_1, t_2, t_3, A_1, A_2 and A_3) are the fitting coefficients for the kinetic behaviour that gave the best fit.

points which in our case were set at 2000.

When we probe the sample with particular energy, the excited electron residing at a lower state in CB will jump to higher electronic or vibronic states by absorbing energy from the probe. For example, if the probing energy is 2.43 eV, the electron will jump to a state which is 2.43 eV above its present state in CB. The electrons in these states are not stable and they will eventually come back to the CB edge by either internal conversion (IC) or vibrational relaxations (thermalization) [10]. The photoexcited carriers sitting in higher-order states excited by above band energy will be mostly trapped without thermalization or IC [10]. The lifetime for these states will directly provide the information of the

trap time (t_1). While for the near and below bandgap excitations the carriers do come to CB edge through thermalization and IC and are eventually trapped in defect states. The decay of these trapped carriers will happen non-radiatively in a time that can reach up to 100 s of picoseconds. As there is no signature of the radiative recombination ($S_1 \rightarrow S_0$), the prominent path followed will be through traps. We will be using a model popularly used by previous researches called the rate equation model and its modified version to explain our data [31,48]. As mentioned, it aptly defines the behavior for above or near bandgap excitations. This model (Figs. 9–11) assumes that there is a large density of mid-bandgap states. As our sample is unannealed so we can also adopt

this assumption to describe the behavior of LT-GaAs under different probing and pumping conditions.

All kinetic profile in Figs. 6–8 shows one or more of three different behaviors; a) a sharp rise followed by inversion of ΔA that lasts for few tens of picoseconds and is prominent for energy far greater than E_g , b) inversion lasts for lesser time for energy near E_g , and c) a quick exponential decay without any inversion followed by slow relaxation for lower energy. A sharp rise in ΔA is due to the filling of higher states by the carriers from lower states in CB. This filling is more prominent near 771 nm (edge state) because of the large density of carriers in the edge states due to thermalization and IC and a decrease in band filling effect. Once LT-GaAs film is exposed to optical excitation, it mostly shows a transition from the valence band (VB)-conduction band (CB) and As_{Ga}^0 -CB [11]. Therefore, the concentration of As_{Ga}^+ donor ions basically remains unaffected. The Gallium vacancies (native acceptors) near to valence band will be completely ionized at room temperature by capturing donor electrons from the mid-gap region [11]. Apart from that the pump and probe wavelengths near to defect states will cause an additional increase in the number of ionized states in the mid-band region due to As_{Ga}^0 -CB transition. So, there will be many empty trap states sitting in the middle of the forbidden gap.

The sharp decay of sub-picosecond duration is due to thermalization and subsequently trapping of CB electrons by these empty states [11]. This trap time is a function of pump and probe wavelengths. The table in Figs. 9–11 lists the approximate trap time for above and below E_g pump and visible to NIR probe. These values are calculated through the fitting of the kinetic profile in surface Xplorer software provided by ultrafast systems [49,50].

As seen from the absorption spectra, significant changes occur by probing at slightly above and near the bandgap. Figs. 6 and 9 reveal the dynamics of hot electron coulombic interactions including band filling and bandgap renormalization. The absorption kinetics (Fig. 6(b)) shows a negative dip after a sharp induced absorption peak. The negative dip is an indicator of bandgap renormalization. The interaction between excited carriers reduces the single-particle potential energy, thus, causing a shift in bandgap or bandgap renormalization [40]. On probing near to the bandgap (849 nm) i.e. above (771 nm) and below (856 nm) E_g , a transition of electrons would be observed either from VB to CB or defect states to CB respectively [11]. For example, while probing in the visible range (Fig. 6(a)) (above the bandgap wavelengths), a negative dip in kinetics (Fig. 6(b)) is observed, which is due to the excitation of carriers from VB. The dip is more prominent near 771 nm because ground state electrons can see many empty states near CB edge due to high ESA. Most of the above band excitations to a higher-order state in CB results in direct trapping instead of thermalization to a lower order state in CB [31]. Lifetime parameters along with a model describing the above behavior are shown in Fig. 9. Where, t_1 is trap time which increases (0.128 ps, 0.31 ps, and 0.807 ps) with probing wavelength (603 nm, 692 nm and 771 nm). This is due to the incorporation of the thermalization time of PIA electrons. Also, the percentage of carriers directly getting trapped also decreases due to the saturation of traps by electrons from higher-order states. The time taken to relax back to the ground state is somewhat slow because of presence of As_{Ga}^+ traps and tail states. Trap emptying time or recombination time is calculated by t_2 and t_3 . These two decay times show the presence of two types of defects i.e. tail defect states below the CB and mid-gap defects [51]. The tail states generally are weakly coupled to CB and eventually result in longer decay time for carries (t_3).

For 2.58 eV(480 nm) excitation but NIR region probing (Fig. 7(a)), excitation from a VB state by absorption of 849 nm probe is observed. As mentioned earlier, this behavior is dominated by ESA up to 5 ps, as the probe does not have much energy to excite many electrons from VB and the density of ground state electrons is less because of the above bandgap (480 nm) excitation. For longer wavelengths (1000 nm, 1164 nm and 1356 nm) no (Fig. 7(b)) re-normalisation is observed. The kinetics for these wavelengths consisted of excitation within CB or from

As_{Ga}^0 defects to CB. At 1000 nm longest delay time is observed because 1000 nm corresponds to a tail state. Generally, an event of probe exciting an electron from this tail state will be followed by transition of a VB electron to this empty state but since for this excitation wavelength the density of upper valence band electrons will be negligible, these empty tail states will be filled by electrons decaying from higher-order states in CB. So, $1.25 \text{ ns} \pm 280 \text{ ps}$ is the time electron takes to decay from a tail state at 1000 nm. At 1164 nm and 1356 nm probe, as the kinetics shows fastest decay, so this signal will correspond to the recombination of electrons with holes in defect states i.e. CB- As_{Ga}^0 transition. The transition due to the above bandgap probe and pathways of decay for NIR region is modeled in Fig. 10 along with the time constants obtained from fitting the decay kinetics.

With 0.88 eV(1400 nm) excitation pulse (Figs. 8 and 11), the mid-band defect of CB- As_{Ga}^0 will be perturbed and a transition will happen to CB. So, there is an increase in electron trap states in the mid-band region. This single-photon absorption (1 PA) (linear absorption) from defects will result in trapping of VB electrons as band to band (VB-CB) transitions are negligible. The probe, as mentioned, has a wavelength that covers 850 nm to 1600 nm. So, the NIR probe will carry the information of band excitation (around 849 nm) as well as defect excitation (>900 nm). But because of 1400 nm (low energy) excitation wavelength, the dominance will be of defect excitation (Fig. 11). As the defect states will largely contribute to the excited state electrons. So, the magnitude of absorption will be a function of defect concentration. The kinetics will give a direct calculation of trap emptying time along with the trapping time. Kinetics at 866 nm probe for excitation at 1400 nm in Fig. 8(b), shows ESA dominant bandgap renormalization which shows similar behavior as observed when excitation was 480 nm in Fig. 7(b). A slight increase in this negative absorption is because of VB-CB transition with the absorption of energy from the probe, 2 PA (because of 1400 nm excitation) and a decrease in coulombic screening because of less density of excited electrons in CB. Trapping time (t_1) (Fig. 11) is determined to be 0.56 ps since the states are saturated with 1 PA and tail state (866 nm) absorption from VB, so the percentage contributing of carriers to this time is 65% only. The decay time from these traps is $t_2 = 6.5 \text{ ps}$ (mid gap) and $t_3 = 91.5 \text{ ps}$ (tail) and the remaining percentage of charge carriers (3.9%) decay by an infinite time constant (Fig. 11). This very long lifetime corresponds to tail states that lie close to CB edge. With 866 nm probe (near bandgap) and 1400 nm excitation, three different decays corresponding to three different trap states are observed; a) mid gap ($t_2 = 6.5 \text{ ps}$), b) tail state closest to band edge ($t > 8 \text{ ns}$) and c) traps that lie in between these two ($t_3 = 91.5 \text{ ps}$). A probing at 989 nm clearly incorporates the behavior of a tail state which has trapped a VB electron. The main transitions that happen at this probe wavelength are VB-CB (2 PA), mid traps to CB (1400 nm excitation i.e. single photon), tail states to CB and VB to empty tail states (Fig. 11). The transitions involving tail states tend to increase the lifetime. The concentration of carriers getting trapped in the trap states rise due to the contribution from two traps levels; firstly the mid-gap-defect states and secondly the tail states. As seen in Fig. 11, it is observed that 3.90% of excited carriers decay in 0.35 ps time (t_1) indicating quickest trap time. While t_2 (18.6 ps) is first trap state decay while t_3 (280 ps)is second trap state (tail) decay time. The kinetics at 1185 nm wavelength mostly shows an excitation from defects (As_{Ga}^0) and subsequent annihilation of electrons to defects ($t_1 = 0.55 \text{ ps}$) along with the decay of 2 PA and single-photon excitation to VB ($t_2 = 19.1 \text{ ps}$). Thus, at 1185 nm trap emptying time is t_2 and which is faster than 989 nm state because of no trapping of VB electrons by tail states. Near edge traps hold small contribution (0.49% and 1.6% respectively) in decay kinetics of 989 nm and 1185 nm states.

4. Summary and conclusions

In conclusion, we have presented a comprehensive explanation of the pathways of carrier decay with above (2.58 eV) and below (0.88 eV) E_g excitation condition along with variable probing at wavelengths ranging

from visible to NIR (0.88 eV–2.75 eV) for semi-insulating LT-GaAs film grown by MBE. The thickness and crystallinity of film are been confirmed by ellipsometry, GI-XRD and Raman spectroscopy. The presence of defect states is well evident from the data obtained by Hall measurement and Raman (TO peak) as well as from the lifetime calculated in UFTS. The films grown are ~43 nm thick and crystalline with LO and TO center frequency at 8.77 THz and 8.03 THz respectively and having a high resistivity value of about $2.53 \times 10^3 \Omega\text{-cm}$. Steady-state absorption showed a residual absorption due to isolated defects (As_Ga^0) for longer wavelength ($E_\text{u} = 1068.9 \text{ nm}$). The same was confirmed from UFTS data for probing above 1.24 eV. In UFTS, a drastic change in kinetics profile and lifetime of relaxation with a change in excitation and probe wavelengths is observed. The presence and dominance of specific coulomb interactions (such as band filling and bandgap renormalization) were revealed on probing above and around the bandgap. Probing below the bandgap, however, identified the distribution and contribution of defects on carrier lifetime and optical behavior of LT-GaAs. Maximum bandgap renormalization was observed for near bandgap probing while the band filling effect was more dominant for above band excitation. Shorter wavelengths captured the behavior of ionized defects (As_Ga^+) while in longer wavelength (higher than 1000 nm) absorption profile gave information about neutral defect states (As_Ga^0). Calculated trapping time was in ~128 fs - ~807 fs range for all probing wavelengths. The time of relaxation to ground state varied over a wide range from ~1.38 ps to ~1.25 ns depending on the trapping state. Tail states near the CB (866 nm) showed shorter decay time ($t_3 = 91.5 \text{ ps}$) than tail states slightly away (989 nm) ($t_3 = 280 \text{ nm}$). At 1000 nm the longest decay time (1.25 ns) was observed. Above 1000 nm mid-gap defects showed their effect and reduced the overall recombination time. This indicates that the trap emptying time is also a function of probing wavelength in addition to growth conditions and annealing temperature and time. This study provides a comprehensive insight into the carrier dynamic of LT-GaAs which can be useful in designing and development of new and advanced optoelectronic and photonic devices.

Declaration of competing interest

The authors declare that they have no known competing financial interests or personal relationships that could have appeared to influence the work reported in this paper.

Acknowledgements

The authors will like to thank CSIR-NPL and IITBNF for providing instrumental facilities required for this work for Dr. Nita Dilawar for Raman Spectroscopy, Dr. K.K. Maurya for GI-XRD, Dr. Ritu Srivastava for Ellipsometry, Dr. S.P. Singh for UV-VIS Spectroscopy. One of the authors, Nikita Vashistha, would like to thank UGC for providing student research fellowship.

Appendix A. Supplementary data

Supplementary data to this article can be found online at <https://doi.org/10.1016/j.physb.2020.412441>.

References

- [1] J. Yoon, S. Jo, I.S. Chun, I. Jung, H. Kim, M. Meitl, E. Menard, X. Li, J.J. Coleman, U. Paik, J.A. Rogers, GaAs photovoltaics and optoelectronics using releasable multilayer epitaxial assemblies, *Nature* 465 (2010) 329–334, <https://doi.org/10.1038/nature09054>.
- [2] N. Bar-chaim, S. Margalit, A. Yariv, I. Ury, GaAs integrated optoelectronics, *IEEE Trans. Electron. Dev.* 29 (1982) 1372–1381, <https://doi.org/10.1109/T-ED.1982.20885>.
- [3] O. Wada, Optoelectronic integration based on GaAs material, *Opt. Quant. Electron.* 20 (1988) 441–474, <https://doi.org/10.1007/BF00635747>.
- [4] A.W. Bett, F. Dimroth, G. Stollwerck, O.V. Sulima, III-V compounds for solar cell applications, *Appl. Phys. Mater. Sci. Process* 69 (1999) 119–129, <https://doi.org/10.1007/s00399000062>.
- [5] M. Bosi, C. Pelosi, The potential of III-V semiconductors as terrestrial photovoltaic devices, *Prog. PHOTOVOLTAICS Res. Appl. Prog.* 15 (2007) 51–68, <https://doi.org/10.1002/pip>.
- [6] J.W. Lee, H. Shichijo, H.L. Tsai, R.J. Matyi, Defect reduction by thermal annealing of GaAs layers grown by molecular beam epitaxy on Si substrates, *Appl. Phys. Lett.* 50 (1987) 31–33, <https://doi.org/10.1063/1.98117>.
- [7] N. Chand, R. People, F.A. Baiochi, K.W. Wecht, A.Y. Cho, Significant improvement in crystalline quality of molecular beam epitaxially grown GaAs on Si (100) by rapid thermal annealing, *Appl. Phys. Lett.* 49 (1986) 815–817, <https://doi.org/10.1063/1.97556>.
- [8] M. Luysberg, H. Sohn, A. Prasad, P. Specht, Z. Lilienthal-Weber, E.R. Weber, J. Gebauer, R. Krause-Rehberg, Effects of the growth temperature and As/Ga flux ratio on the incorporation of excess as into low temperature grown GaAs, *J. Appl. Phys.* 83 (1998) 561–566, <https://doi.org/10.1063/1.366723>.
- [9] U. Siegner, R. Fluck, G. Zhang, U. Keller, Ultrafast high-intensity nonlinear absorption dynamics in low-temperature grown gallium arsenide, *Appl. Phys. Lett.* 69 (1996) 2566–2568, <https://doi.org/10.1063/1.117701>.
- [10] P.W.E. Smith, S.D. Benjamin, H.S. Loka, Tailoring of trap-related carrier dynamics in low-temperature-grown GaAs, *Appl. Phys. Lett.* 71 (1997) 1156–1158, <https://doi.org/10.1063/1.119852>.
- [11] M. Kaminska, Z. Lilienthal-Weber, E.R. Weber, T. George, J.B. Kortright, F.W. Smith, B.Y. Tsaur, A.R. Calawa, Structural properties of As-rich GaAs grown by molecular beam epitaxy at low temperatures, *Appl. Phys. Lett.* 54 (1989) 1881–1883, <https://doi.org/10.1063/1.101229>.
- [12] D.C. Look, Molecular beam epitaxial GaAs grown at low temperatures, *Thin Solid Films* 231 (1993) 61–73, [https://doi.org/10.1016/0040-6090\(93\)90703-R](https://doi.org/10.1016/0040-6090(93)90703-R).
- [13] J.F. Whitaker, Optoelectronic applications of LTMBE III-V materials, *Mater. Sci. Eng. B* 22 (1993) 61–67, [https://doi.org/10.1016/0921-5107\(93\)90224-b](https://doi.org/10.1016/0921-5107(93)90224-b).
- [14] M. Missous, I. Kostakis, D. Saeedkia, Long wavelength low temperature grown GaAs and InP-based terahertz photoconductors devices, *IEEE Sensor. J.* 13 (2012) 63–71, <https://doi.org/10.1109/jsen.2012.2224332>.
- [15] O.M. Abdulmunem, K.I. Hassoon, J. Völkner, M. Mikulics, K.I. Gries, J.C. Balzer, Photoconductive LT-GaAs terahertz antennas: correlation between surface quality and emission strength, *J. Infrared, Millim. Terahertz Waves* 38 (2017) 574–582, <https://doi.org/10.1007/s10762-016-0353-y>.
- [16] L.R. Brovelli, U. Keller, T.H. Chiu, Design and operation of antiresonant Fabry-Perot saturable semiconductor absorbers for mode-locked solid-state lasers, *J. Opt. Soc. Am. B* 12 (1995) 311, <https://doi.org/10.1364/josab.12.000311>.
- [17] T. Muratani, T. Shimano, S. Mitsui, Growth temperature dependence in molecular beam epitaxy of gallium arsenide, *J. Cryst. Growth* 45 (1978) 302–308, [https://doi.org/10.1016/0022-0248\(78\)90453-0](https://doi.org/10.1016/0022-0248(78)90453-0).
- [18] G.L. Witt, LTMBE GaAs: present status and perspectives, *Mater. Sci. Eng. B* 22 (1993) 9–15, [https://doi.org/10.1016/0921-5107\(93\)90215-9](https://doi.org/10.1016/0921-5107(93)90215-9).
- [19] W.C. Lee, T.M. Hsu, J.I. Chyi, G.S. Lee, W.H. Li, K.C. Lee, Characterization of low temperature GaAs grown by molecular beam epitaxy, *Appl. Surf. Sci.* 92 (1996) 66–69, [https://doi.org/10.1016/0169-4332\(95\)00204-9](https://doi.org/10.1016/0169-4332(95)00204-9).
- [20] S. Fleischer, C.D. Beling, S. Fung, W.R. Nieveen, J.E. Squire, J.Q. Zheng, M. Missous, Structural and defect characterization of GaAs and Al_xG_{1-x}As grown at low temperature by molecular beam epitaxy, *J. Appl. Phys.* 81 (1997) 190–198, <https://doi.org/10.1063/1.364105>.
- [21] P.W.E. Smith, S.D. Benjamin, Materials for all-optical devices, *Opt. Eng.* 34 (1995) 189–194, <https://doi.org/10.1117/12.188341>.
- [22] F.W. Smith, A.R. Calawa, C.L. Chen, M.J. Manfra, L.J. Mahoney, New MBE buffer used to eliminate backgating in GaAs MESFET's, *IEEE Electron. Device Lett.* 9 (1988) 77–80, <https://doi.org/10.1109/55.2046>.
- [23] Z. Lilienthal-Weber, H.J. Cheng, S. Gupta, J. Whitaker, K. Nichols, F.W. Smith, Structure and carrier lifetime in LT-GaAs, *J. Electron. Mater.* 22 (1993) 1465–1469, <https://doi.org/10.1007/BF02650000>.
- [24] Z. Lilienthal-Weber, W. Swider, K.M. Yu, J. Kortright, F.W. Smith, A.R. Calawa, Breakdown of crystallinity in low-temperature-grown GaAs layers, *Appl. Phys. Lett.* 58 (1991) 2153–2155, <https://doi.org/10.1063/1.104990>.
- [25] X. Liu, A. Prasad, W.M. Chen, A. Kurpiewski, A. Stoscheck, Z. Lilienthal-Weber, E. R. Weber, Mechanism responsible for the semi-insulating properties of low-temperature-grown GaAs, *Appl. Phys. Lett.* 65 (1994) 3002–3004, <https://doi.org/10.1063/1.112490>.
- [26] H. Némec, A. Pashkin, P. Kužel, M. Khazan, S. Schnüll, I. Wilke, Carrier dynamics in low-temperature grown GaAs studied by terahertz emission spectroscopy, *J. Appl. Phys.* 90 (2001) 1303–1306, <https://doi.org/10.1063/1.1380414>.
- [27] M.O. Manasreh, D.C. Look, K.R. Evans, C.E. Stutz, Infrared absorption of deep defects in molecular-beam-epitaxial GaAs layers grown at 200 C: Observation of an EL 2-like defect, *Phys. Rev. B* 41 (1990) 10272–10275, <https://doi.org/10.1103/physrevb.41.10272>.
- [28] M. Toufella, P. Puech, R. Carles, E. Bedel, C. Fontaine, A. Claverie, G. Benassayag, Diameter of as clusters in LT-GaAs by Raman spectroscopy, *J. Appl. Phys.* 85 (1999) 2929–2933, <https://doi.org/10.1063/1.369058>.
- [29] A.I. Lobad, Y. Kostoulas, G.W. Wicks, P.M. Fauchet, Hot carrier thermalization dynamics in low-temperature-grown III-V semiconductors, in: K. Hess (Ed.), *Hot Carriers Semicond.*, Springer US, New York, 1996, pp. 97–99, <https://doi.org/10.1007/978-1-4613-0401-2>.
- [30] K.A. McIntosh, K.B. Nichols, S. Vergheese, E.R. Brown, Investigation of ultrashort photocarrier relaxation times in low-temperature-grown GaAs, *Appl. Phys. Lett.* 70 (1997) 354–356, <https://doi.org/10.1063/1.118412>.

- [31] S.D. Benjamin, H.S. Loka, A. Othonos, P.W.E. Smith, Ultrafast dynamics of nonlinear absorption in low-temperature-grown GaAs, *Appl. Phys. Lett.* 68 (1996) 2544, <https://doi.org/10.1063/1.116178>.
- [32] A.J. Lochtefeld, M.R. Melloch, J.C.P. Chang, E.S. Harmon, The role of point defects and arsenic precipitates in carrier trapping and recombination in low-temperature grown GaAs, *Appl. Phys. Lett.* 69 (1996) 1465–1467, <https://doi.org/10.1063/1.116909>.
- [33] S.D. Benjamin, H.S. Loka, P.W.E. Smith, Tailoring of low-temperature MBE-grown GaAs for ultrafast photonic devices, *Can. J. Phys.* 74 (1996) S64–S68, <https://doi.org/10.1139/p96-834>.
- [34] V. Ortiz, J. Nagle, A. Alexandrou, Influence of the hole population on the transient reflectivity signal of annealed low-temperature-grown GaAs Influence of the hole population on the transient reflectivity signal of annealed low-temperature-grown GaAs, *Appl. Phys. Lett.* 80 (2002), <https://doi.org/10.1063/1.1463209>.
- [35] S. Gupta, J.F. Whitaker, Structure and carrier lifetime in LT-GaAs, *J. Electron. Mater.* 22 (1993), <https://doi.org/10.1007/BF02650000>.
- [36] S.D. Benjamin, A. Othonos, P.W.E. Smith, Large ultrafast optical nonlinearities in As-rich GaAs, *Electron. Lett.* 30 (1994) 1704–1706, <https://doi.org/10.1049/el:19941154>.
- [37] X.Q. Zhou, H.M. Van Driel, G. Mak, Femtosecond kinetics of photoexcited carriers in germanium, *Phys. Rev. B* 50 (1994) 5226–5230, <https://doi.org/10.1103/PhysRevB.50.5226>.
- [38] C.Y. Sung, H.H. Wang, T.B. Norris, J.F. Whitaker, Ultrafast electron and hole trapping times and defect band saturation dynamics in low-temperature-grown GaAs, *CLEO, 1996*, p. 454.
- [39] J. Sjakste, N. Vast, G. Barbarino, M. Calandra, F. Mauri, J. Kanasaki, H. Tanimura, K. Tanimura, Energy relaxation mechanism of hot-electron ensembles in GaAs: theoretical and experimental study of its temperature dependence, *Phys. Rev. B* 97 (2018) 1–9, <https://doi.org/10.1103/PhysRevB.97.0644302>.
- [40] T. Gong, W.L.N. Jr, P.M. Fauchet, Hotcarrier Coulomb Effects in GaAs Investigated by Femtosecond Spectroscopy Around the Band Edge Hot-Carrier Coulomb Effects in GaAs Investigated by Femtosecond Spectroscopy Around the Band Edge, 2713, 1990, pp. 57–60, <https://doi.org/10.1063/1.103808>.
- [41] G. V Hartland, Coherent vibrational motion in metal particles : determination of the vibrational amplitude and excitation mechanism, *J. Chem. Phys.* 116 (2002), <https://doi.org/10.1063/1.1469021>.
- [42] S.H. Lee, H.S. Sim, J. Lee, J.M. Kim, Y.E. Shin, Three temperature model for nonequilibrium energy transfer in semiconductor films irradiated with short pulse lasers, *Mater. Trans.* 47 (2006), <https://doi.org/10.2320/matertrans.47.2835>.
- [43] S.R. Johnson, T. Tiedje, Temperature dependence of the Urbach edge in GaAs, *J. Appl. Phys.* 78 (1995) 5609–5613, <https://doi.org/10.1063/1.359683>.
- [44] I. Studenyak, M. Kranj, M. Kurik, Urbach rule in solid state physics, *Int. J. Optic. Appl.* 4 (2014) 76–83, <https://doi.org/10.5923/j.optics.20140403.02>.
- [45] T.F. Boggess, A.L. Smirl, S.C. Moss, I.W. Boyd, E.W. Van Stryland, Optical limiting in GaAs, *IEEE J. Quant. Electron.* 21 (1985) 488–494, <https://doi.org/10.1109/JQE.1985.1072688>.
- [46] A. Penzkofer, A.A. Bugayev, Two-photon absorption and emission dynamics of bulk GaAs, *Opt. Quant. Electron.* 21 (1989) 283–306, <https://doi.org/10.1007/BF02027300>.
- [47] N. Mouton, M. Sliwa, G. Buntinx, C. Ruckebusch, Deconvolution of femtosecond time-resolved spectroscopy data in multivariate curve resolution . Application to the characterization of ultrafast photo-induced intramolecular proton transfer, *J. El Chemom.* 24 (2010) 424–433, <https://doi.org/10.1002/cem.1315>.
- [48] N.P. Wells, P.M. Belden, J.R. Demers, W.T. Lotshaw, Transient Reflectivity as a Probe of Ultrafast Carrier Dynamics in Semiconductors : A Revised Model for Low-Temperature Grown GaAs Semiconductors : A Revised Model for Low-Temperature Grown GaAs, 073506, 2014, <https://doi.org/10.1063/1.4892868>.
- [49] V. Gupta, V. Bharti, M. Kumar, S. Chand, A.J. Heeger, Polymer-polymer Förster resonance energy transfer significantly boosts the power conversion efficiency of bulk-heterojunction solar cells, *Adv. Mater.* 27 (2015) 4398–4404, <https://doi.org/10.1002/adma.201501275>.
- [50] A. Jana, H.B. Gobze, M. Ishida, T. Mori, K. Ariga, J.P. Hill, F.D. Souza, Zinc porphyrin by metal – ligand coordination to, *Dalton Trans.* 44 (2014) 359–367, <https://doi.org/10.1039/C4DT03157a>.
- [51] I.S. Gregory, Two-trap Model for Carrier Lifetime and Resistivity Behavior in Partially Annealed GaAs Grown at Low Temperature, 2006, pp. 1–8, <https://doi.org/10.1103/PhysRevB.73.195201>.